Acta Crystallographica Section D
Biological Crystallography
ISSN 0907-4449

Three-beam interference is a sensitive measure of the efficacy of macromolecular refinement techniques

Alexei S. Soares,[a] Donald L. D. Caspar,[b] Edgar Weckert,[c] Annie Héroux,[a] Kerstin Hölzer,[a] Klaus Schroer,[a] Johannes Zellner,[c] Dieter Schneider,[a] William Nolan[a] and Robert M. Sweet[a]*

[a]Biology Department, Brookhaven National Laboratory, Upton, NY 11973, USA, [b]Institute of Molecular Biophysics, Florida State University, Tallahassee, FL 32306, USA, and [c]HASYLAB at DESY, Notkestrasse 85, D-22603 Hamburg, Germany

Correspondence e-mail: sweet@bnl.gov

Received 8 May 2003
Accepted 11 July 2003

Triplet phases recorded from insulin crystals were used to measure the improvement of phases during model refinement and to quantify the contribution made by each step in the refinement. Conventional amplitude data were recorded to 1.5 Å resolution from rhombohedral pig insulin crystals using 1.54 Å Cu $K\alpha$ radiation. An initial atomic model and starting phases were obtained from a published structure and the atomic model was refined against the amplitude data using *CNS*. The refined phases were compared with 800 triplet phases that were measured from similar crystals using a three-beam interference technique and 1.1 Å wavelength synchrotron radiation. The solvent region was improved further using a novel density-modification procedure. Calculated triplet phases were obtained from the model after each step in the refinement and were compared with the recorded triplet phases. The average difference between the recorded triplet phases and the calculated triplet phases was used as an unbiased measure of the correctness of the model at each stage in the refinement. The average individual phase error was estimated from discrepancies from triplet phases after each refinement step. Conventional atomic refinement of an approximate starting model reduced the average individual phase error from 21.6 to 14.7°. Improvement of the solvent region, including the difference-map flattening procedure, reduced the individual phase error by a further 2.6°. Modeling the discrete disorder of four amino acids accounted for an additional 0.5° improvement and the final individual phase error was 11.6°.

1. Introduction

The correct fitting of an initial model to an electron-density map is not the conclusion of an X-ray crystallography structure-determination effort; refinement by numerical methods is required. Refinement of an initial model is a laborious computation and frequently requires substantial investment of time and effort. Rapid advances in refinement software and a deepening pool of conventional wisdom for designing effective refinement protocols frequently change the structure-optimization landscape. In this work, we introduce a novel tool for evaluating the efficacy of this increasingly large array of refinement options.

The conventional method for evaluating the usefulness of a particular refinement step is to validate the atomic structure subsequent to the refinement (Dodson *et al.*, 1996; Kleywegt, 2000). Improvement in the *R* factor and free *R* factor between calculated and observed structure-factor moduli (Brünger, 1992), good agreement of stereochemical values with data tabulated from small-molecule work (Engh & Huber, 1991) and improvement in the properties of the electron-density

map (Akker & Hol, 1998; Mowbray *et al.*, 1999; Terwilliger & Berendzen, 1999) are all indicators that the refinement protocol in question was effective. Refinement methods are evaluated indirectly using characteristics of the model because it is not normally possible to measure phases as accurately as amplitudes or stereochemical values.

The experimental phase information available during most structure-determination efforts does not extend to sufficiently high-frequency terms and is not accurate enough to directly evaluate the value of the final refinement stages. When it can be measured, highly accurate phase information is very useful. Brünger's group published accurate and complete MAD phases extending to 1.8 Å from mannose-binding protein (Burling *et al.*, 1996). The data were intended specifically to evaluate new refinement protocols and to observe directly the extent of improvement in the model phases using new refinement protocols. The authors reported a 21° estimated experimental error for the phase data. The mean reported phase difference between experimental phases and phases calculated from the mannose-binding protein model was 27.3°. In contrast, our group obtained direct phase information using a three-beam diffraction technique with a 12° estimated experimental error and 23.4° difference between experimental triplet phases and triplet phases calculated from our model (see §4). Note that if all of this 23.4° discrepancy is considered to come equally from each of the three phases, combined in quadrature, this represents a 13.5° total phase error from each reflection in the triplet, about half that observed from the Burling experiment (see also §3.3 and §3.4). These three-beam phases match the model values remarkably well.

Density-modification (DM) schemes frequently cannot benefit from explicit atomic models since DM focuses on interstitial solvent or highly disordered regions of the unit cell where such atomic models are inappropriate. Consequently, density-modification schemes suffer disproportionately from over-fitting and model-bias problems (Cowtan, 1999; Cowtan & Main, 1996) and their effectiveness cannot be judged by improvements in the stereochemistry or other properties of the atomic model. Other experimental sources of phase information such as MIR or MAD rely on an explicit atomic model of one or a few strong diffractors. They are not ideal for phasing low-resolution reflections because a few strongly scattering atoms contribute only weakly to most low-resolution terms. The disordered regions of the protein and the solvent, which generally constitute at least half of the total number of scattering electrons, contribute substantially to these low-resolution terms (Badger & Caspar, 1991; Podjarny & Urzhumstev, 1997).

In the present work, our aim was to examine the efficacy of each step in the conventional refinement of rhombohedral insulin and also to investigate a novel difference-map flattening density-modification protocol (described in §3.5) for improving the quality of the solvent model (Yu *et al.*, 1999). The project required extremely accurate and totally model-independent phase information drawn from regions of reciprocal space between 20 and 2.0 Å. Such remarkably accurate and model-independent phases can be obtained with a three-beam interference experiment (Weckert & Hümmer, 1997; Shen, 1999). Because the number of reflections from a protein crystal is so large, it was possible to spot-check the improvement in phases in each region of reciprocal space with good statistics using only a fraction of the possible reflections.

Three-beam interference presents several advantages relative to alternative methods for tracking phase improvement during a refinement procedure. Firstly, the experimental error in triplet phases is small compared with the errors in phases calculated from refined models. Secondly, only a limited number of triplet phases need to be measured when the method is used to validate a structure, which is less demanding than using triplet phases to determine a structure from scratch (Hölzer *et al.*, 2000; Weckert *et al.*, 1999). Thirdly, the phase information is completely model-independent. This last advantage is particularly critical when evaluating density-modification schemes.

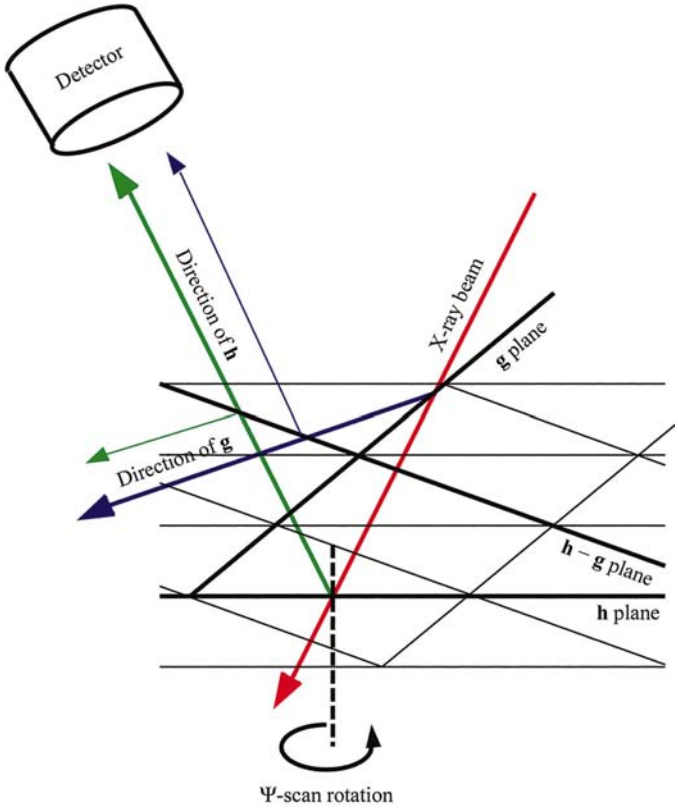

Figure 1
Graphical representation of a three-beam case. The lattice planes of **g**, of **h** and of **h** − **g** are shown in black and the incident beam is shown in red. The primary wave **h** is shown in green, as is the weaker *umweg* wave, which is the second reflection of the **h** wave from the (**h** − **g**) planes in the **g** diffracted-beam direction. The secondary wave **g** is shown in blue, as is the weaker *umweg* wave in the **h** direction. Strong waves are shown in bold. The experimentally measured quantity is the intensity in the direction of **h** as **g** is brought in and out of the reflecting condition by a sample rotation called a Ψ scan. The rotation axis of the Ψ scan is illustrated with dotted lines. The *umweg* wave in the direction of the **h** diffracted beam will interfere with the primary wave **h** (fine blue interferes with bold green). The observed intensity change will depend on the relative amplitudes and the difference between the phase of the *umweg* wave and the phase of **h**: $\varphi(\mathbf{g}) + \varphi(\mathbf{h} - \mathbf{g}) - \varphi(\mathbf{h})$. Typical intensity profiles are shown in Fig. 2.

2. Three-beam interference

Experimental triplet phases for a protein structure were first published in 1991 from crystals of myoglobin (Hümmer *et al.*, 1991) and hemoglobin (Chang *et al.*, 1991) using techniques for measuring triplets one at a time that were developed with small molecules (Hümmer *et al.*, 1990; Weckert & Hümmer, 1990). Measuring phases one at a time is accurate but laborious and time-consuming. To provide a viable alternative to established phasing methods, the more rapid 'reference-beam' method for measuring multiple triplets simultaneously was recently proposed by Shen (1998*b*). The reference-beam method has been successfully used to phase protein structures (Shen, 1998*a*; Shen *et al.*, 2000; Chao *et al.*, 2002), including a recent report of almost complete rapid phasing of tetragonal lysozyme that suggests that a viable alternative for routine solution of the phase problem may be around the corner (Shen & Wang, 2003).

A theoretical treatment of the three-beam diffraction method is necessarily lengthy (Weckert & Hümmer, 1997) and only a brief description is given here. In a conventional crystallography experiment based on the so-called rotation method, hundreds of reflections are excited on each diffraction image, yielding data frames containing a large number of spots. The integrated intensities are treated as independent of each other. However, to the extent that several reflections are diffracting at each position of the crystal during the rotation, every excited reflection modulates the intensity of every other excited reflection indirectly by the interference of a third non-excited *umweg* (detour) reflection. In a conventional crystallography experiment, this interference is a nuisance (when it happens in a silicon or germanium monochromator crystal, it is called a glitch). A three-beam interference experiment is designed to exploit this interference phenomenon in order to determine triplet phases $\Phi = \varphi(\mathbf{g}) + \varphi(\mathbf{h} - \mathbf{g}) - \varphi(\mathbf{h})$, where $\mathbf{h}$ and $\mathbf{g}$ are the reciprocal-space vectors of two arbitrary reflections (please refer to Fig. 1). Notice that since $-\varphi(\mathbf{h}) = \varphi(-\mathbf{h})$ this is really a sum of phases of reflections, the sum of whose indices is zero. This is the classic 'triplet' phase invariant used in all direct-phasing methods.

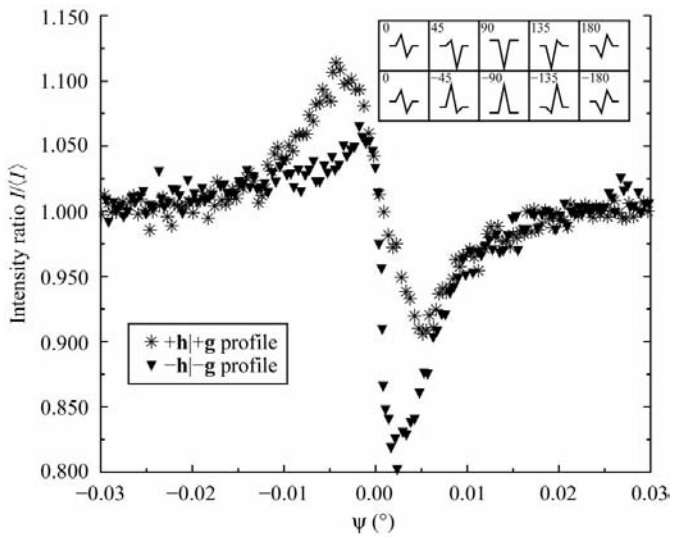

Figure 2
Interference profiles for $+\mathbf{h}|+\mathbf{g}$ and $-\mathbf{h}|-\mathbf{g}$ of a typical three-beam case. The phase-independent contributions are symmetric and the phase-dependent contributions are antisymmetric. Consequently, by adding the $+\mathbf{h}|+\mathbf{g}$ profile to the inverse of the $-\mathbf{h}|-\mathbf{g}$ profile, only the phase-dependent contribution remains. This increases the accuracy of the phasing. The $-\mathbf{h}|-\mathbf{g}$ profile has already been inverted for convenience (about both the x and y axes). Data points measured for the three-beam case $+\mathbf{h}|+\mathbf{g}$ are shown as stars and data points for the three-beam case $-\mathbf{h}|-\mathbf{g}$ are indicated by triangles. Each shape corresponds to a unique triplet-phase value. For this measurement $\mathbf{h}$ was (−25, 1, −2), $\mathbf{g}$ was (−7, 2, 0) and the estimated triplet phase was 20°. The triplet phase calculated from one refined model was 30° ($\varphi_{\mathbf{g}} = 188°$, $\varphi_{\mathbf{h}-\mathbf{g}} = -1°$, $-\varphi_{\mathbf{h}} = 203°$) and the triplet phase calculated from a second refined model was also 30° ($\varphi_{\mathbf{g}} = 186°$, $\varphi_{\mathbf{h}-\mathbf{g}} = -5°$, $-\varphi_{\mathbf{h}} = 209°$). Triplet phases were determined from the experimental profiles by averaging a visual phase estimate (see inset at upper right) with a computer phase estimate (see §3.3).

Three-beam interference profiles are measured by maintaining one reciprocal-space node in a reflecting position and bringing a second node into and then out of the reflection position. The node that is maintained on the sphere of reflection is called the primary reflection $\mathbf{h}$ and the node that is moved through the sphere of reflection is called the secondary reflection $\mathbf{g}$. Maximum interference occurs when the incident beam optimally excites both $\mathbf{h}$ and $\mathbf{g}$. This is called a three-beam case (see Fig. 1). In a three-beam case, the primary reflection $\mathbf{h}$ is diffracted into the direction of the secondary reflection $\mathbf{g}$ by the difference vector $\pm(\mathbf{h} - \mathbf{g})$. Similarly, the secondary reflection $\mathbf{g}$ is diffracted into the direction of the primary reflection $\mathbf{h}$ by $\pm(\mathbf{h} - \mathbf{g})$. Consequently, $\mathbf{h}$ and $\mathbf{g}$ interfere with each other *via* $(\mathbf{h} - \mathbf{g})$. The interference between the strong $\mathbf{h}$ wave and the weaker double-diffracted $\mathbf{h} - \mathbf{g}$ wave results in a change in the measured intensity of the $\mathbf{h}$ wave while the $\mathbf{g}$ wave traverses the sphere of reflection. The interference between the two waves depends on the difference between their phases. There is a unique correspondence between every possible phase difference and the shape of the interference profile. Consequently, the phase difference can be obtained from the interference profile.

Since the *umweg* wave is doubly diffracted from both the $\mathbf{g}$ and the $\mathbf{h} - \mathbf{g}$ reciprocal-lattice planes, the phase of the *umweg* wave is $\varphi(\mathbf{g}) + \varphi(\mathbf{h} - \mathbf{g})$ and the phase of $\mathbf{h}$ is $\varphi(\mathbf{h})$. Interference effects depend on the difference between the phases of the two waves Φ,

$$\Phi = \varphi(\mathbf{g}) + \varphi(\mathbf{h} - \mathbf{g}) - \varphi(\mathbf{h}). \quad (1)$$

Since the interference profile can be observed experimentally, the phase difference Φ can be measured. To minimize phase-independent effects, we combined the $+\mathbf{h}|+\mathbf{g}$ interference profile with the $-\mathbf{h}|-\mathbf{g}$ profile. Because phase-independent effects are symmetric and phase-dependent effects are antisymmetric (Weckert & Hümmer, 1990), the combined profile in general preserves only the phase-dependent effects and is more accurate (Fig. 2).

3. Methods

Our three-beam data were measured using an unfocused X-ray beam at NSLS beamline X26-C; the only optical element in the beam was the channel-cut monochromator. The focusing mirror normally employed by the beamline was moved out of the beam path prior to data collection to produce a beam that was nearly parallel at the specimen. Previous three-beam experiments have made use of wavelength-tunable beams. The tunability allows one to isolate three-beam cases from their neighbors. We found it was adequate to select a fixed wavelength of 1.1 Å using the (111) planes from the silicon monochromator.

Triplet phases were measured by superposing 15–30 passes of the secondary reflection through the reflecting condition. Triplet phases were used only when both the $+\mathbf{h}|+\mathbf{g}$ and the $-\mathbf{h}|-\mathbf{g}$ profiles were interpretable. For protein crystals, superposition of three-beam interference profiles cannot be avoided owing to the very dense reciprocal lattice. To measure the interference reliably, the minimum required angular separation in Ψ between the desired $\mathbf{g}$ vector and strong neighboring $\mathbf{g}'$ vectors was 0.02°. To obtain a representative sample of reciprocal space, 800 triplet phases were measured with $\mathbf{h}$, $\mathbf{g}$ and $\mathbf{h}-\mathbf{g}$ between 20 and 2.0 Å (Fig. 3). These were all relatively strong reflections, with the amplitudes of $\mathbf{g}$ and $\mathbf{h}-\mathbf{g}$ stronger than $\mathbf{h}$. Most triplets had one reflection near to 10 Å resolution and one near 4 Å resolution to accentuate the importance of the solvent model in the phases. The triplet phases were used to measure the efficacy of each step in the conventional refinement of an initial atomic model using *CNS* (Brünger *et al.*, 1998; Collaborative Computational Project, Number 4, 1994). The difference-map flattening procedure was also evaluated using the triplet data.

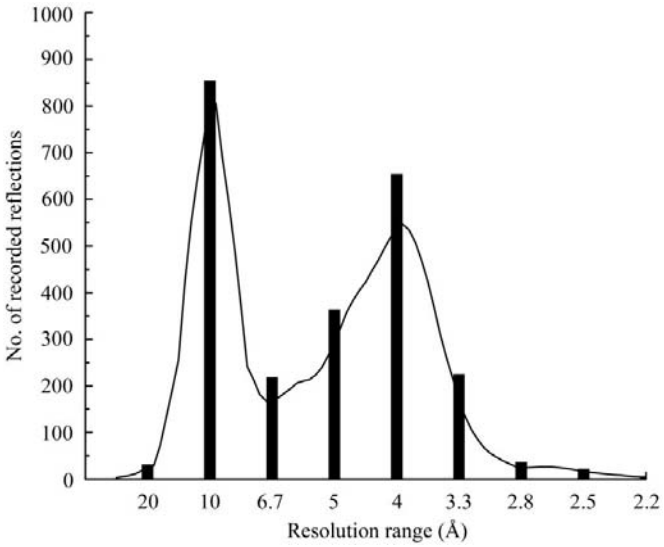

Figure 3
Reciprocal-space distribution of 800 measured triplet phases. The number of reflections in each resolution range for which triplet-phase data were recorded is shown. These represent all three members of the triplets measured ($\mathbf{h}$, $\mathbf{g}$ and $\mathbf{h}-\mathbf{g}$). The bars show the number of reflections in bins with a width of 0.05 Å^{-1}. The continuous curve is generated by placing a small Gaussian of unit volume at each resolution corresponding to a measured reflection.

3.1. Rhombohedral insulin crystals

Triplet phases can be measured from crystal samples with low mosaic spread, large size and high tolerance to X-ray exposure at room temperature. In low-salt conditions and in the presence of a divalent cation, insulin forms suitable crystals in space group *R*3, with unit-cell parameters $a = b = 82.5$, $c = 34.1$ Å, $\alpha = \beta = 90$, $\gamma = 120°$. The crystals were grown by dissolving 0.025 g pig insulin in crystallizing solution (200 ml 0.02 *M* HCl, 100 ml 0.20 *M* sodium citrate, 60 ml acetone, 20 ml H_2O and 20 ml 0.12 *M* $ZnSO_4$) at 313 K and allowing the solution to cool slowly to 293 K. There are two insulin monomers per asymmetric unit (chains A and B form the first monomer and chains C and D form the second, quasi-symmetric monomer). Room-temperature data were collected from rhombohedral insulin crystals with mosaic spreads of ∼0.006°, volumes of ∼0.5 mm^3, and ∼24 h survival in the unfocused beam. The mosaic spread was measured using the 'full-width at half-maximum' standard (Fig. 4). Cryogenic temperatures could not be used to increase survival because freezing drastically increased the mosaic spread.

Insulin has been the focus of solvent-mapping efforts using difference-map flattening (Badger, 1993). In rhombohedral insulin crystals, the HisB10 on each subunit of a quasi-symmetric dimer forms a hydrogen bond with a Zn atom located on the threefold axis. The resulting trimer of dimers surrounds a large isolated cavity bounded on each end by a Zn atom. It is usually possible to model substantially all the electron density in the cavity as either ordered or discretely disordered water molecules. The presence of this ordered cavity and the small volume fraction of bulk solvent (25%) make rhombohedral insulin a useful model for explaining the static and dynamic solvation of protein molecules (Blundell *et al.*, 1972; Wlodawer *et al.*, 1989).

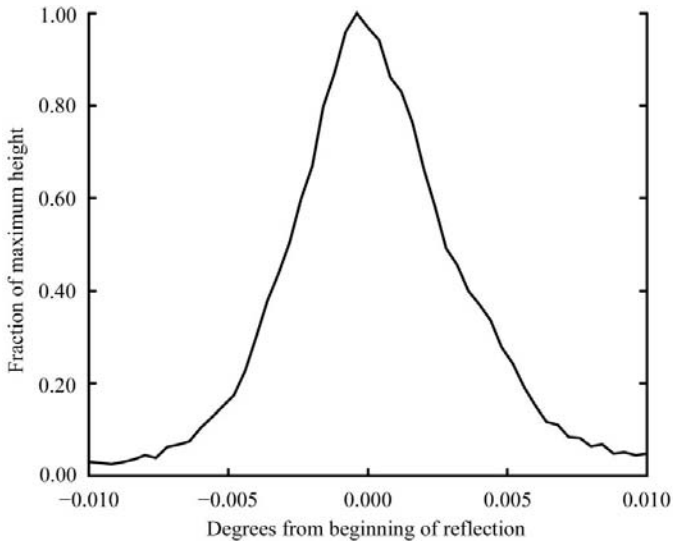

Figure 4
Rocking curve for rhombohedral insulin reflections. A good-quality reflection is illustrated, the $\mathbf{h}$ (−25, 1, −2) reflection from Fig. 2. The full-width at half-maximum (FWHM) is 0.005°.

Table 1
Data-reduction and refinement statistics are shown for two rhombohedral zinc insulin X-ray data sets labeled set *A* and set *B*.

The two data sets were refined independently using the same strategy from the same starting model. Results are shown for refinement up to step (iii) (see §3.2). The free *R* factors are more uncertain than usual because only 2% of the data were reserved for validation.

Insulin data set	*A*	*B*
Space group	*R*3, No. 146	*R*3, No. 146
Unit-cell parameters (Å)	$a = b = 82.6$, $c = 34.0$	$a = b = 82.5$, $c = 34.1$
Resolution (Å)	1.55	1.50
Unique reflections	11979	12678
Observational redundancy	3.6	5.0
R_{sym}(%)	4.2	7.8
Completeness (%)	97.6	95.5
R_{sym} to 2 Å (%)	3.1	6.6
Completeness to 2 Å (%)	100	100
R_{factor} (%)	19.1	19.1
R_{free} (%)	21.3	20.8
R.m.s deviations from ideal		
Bond lengths (Å)	0.005	0.005
Bond angles (°)	1.10	1.11
No. of protein atoms	806	806
No. of water molecules	77	75
Average *B* factor (Å^2)		
Protein atoms	22.9	23.0
Water molecules	35.5	35.1

3.2. Refinement strategy

Amplitude data extending to 1.5 Å resolution were recorded from crystals of rhombohedral insulin for use in conventional refinement and density modification. Room-temperature amplitude data were recorded from two crystals using 1.54 Å Cu $K\alpha$ X-ray radiation from a rotating-anode source. A high-angle data set was obtained using 60 oscillations of 2° and an overlapping low-angle data set was recorded separately with a shorter exposure time and a longer sample-to-detector distance. Amplitudes and phases were calculated after each of five refinement steps.

(i) An initial atomic model and starting phases were obtained from a published structure (Blundell *et al.*, 1972). All water molecules were discarded and alternate conformations were not used.

(ii) Water molecules were built into the model with a short concomitant energy minimization using *CNS*. Waters were built in two stages with a σ cutoff of 3.0 and a maximum temperature factor 50 Å^2. Temperature factors and occupancies of all atoms were refined using *CNS* after water building.

(iii) An explicit flat solvent model was then added as required for application of difference-map flattening.

(iv) Difference-map flattening was used to improve the quality of the solvent region. No changes were made to the density inside the molecular envelope or to the atomic water molecules from step (ii).

(v) Two residues in the B chain and two residues in the D chain were modeled as discretely disordered. Each alternative conformation had equal 50% occupancy. The disordered side chains were GluB21, ArgB22, GluD21 and LysD29.

Because the published starting structure was of high quality, the total reduction in the discrepancy between the measured and the calculated triplet phases was only 4.7° (from 28.1° before refinement to 23.4° after refinement). Therefore, to illustrate the effects of improving a poor starting structure typically available when a model is first built into experimental electron density, we used torsional molecular dynamics, unconstrained by data, to introduce 0.60 Å r.m.s. error into the published model prior to refinement (Rice & Brünger, 1994).

To improve the accuracy of our results, both the conventional refinement and the density modification were performed twice against different amplitude data. The average of the two refinements is reported. Both amplitude data sets were 100% complete to 2.0 Å, with symmetry *R* values of 4.2% (24.1% in the last shell) and 7.8% (17.9% in the last shell), respectively. The data-reduction and refinement statistics are shown in Table 1. The triplet data were not used for conventional refinement and were not involved in the difference-map flattening procedure. Consequently, the agreement between the recorded triplet phases and the triplet phases calculated after each step in the refinement was an accurate and model-free method for evaluating the effectiveness of each stage in the refinement.

3.3. Estimating phasing uncertainty

The average difference between measured triplet phases and triplet phases calculated from the optimum model was 23.4° (Fig. 5). This 23.4° difference is composed of independent contributions from experimental error in the triplet measurements and from the effect of the incorrectness of the model on the **h**, **g** and **h** − **g** reflections. Refinement of a trial starting model with known 0.60 Å r.m.s. error against simu-

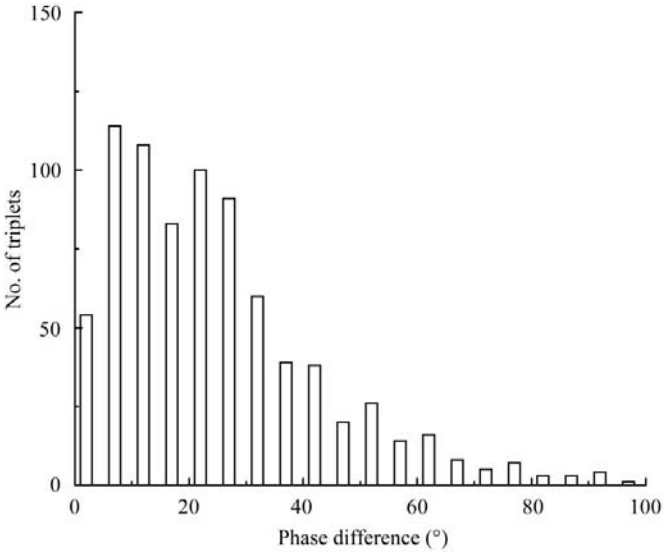

Figure 5
Distribution of discrepancies between measured triplet phases and triplet phases calculated from the final rhombohedral insulin model. The average was 23.4°. The difference between measured and observed triplet phases has independent contributions from experimental error in the measurement and from errors in the phases of **h**, **g** and **h** − **g**.

lated noisy data (introduced noise was equivalent to a 6% R factor) converged to a final refined model with triplet-phase error of 20° relative to the known 'true' model (the triplet-phase error prior to refinement was ∼40°). This 20° is a measure of the uncertainty in the model-refinement procedure against data with a noise similar to those used in our experiment.[1] We presume that this uncertainty combines in quadrature with the uncertainty in the experimental measurement of triplet phases to produce the 23.4° average phase difference between the experimentally measured triplet phases and those calculated from the refined model. Therefore, the implied uncertainly in the measured triplet phase, $\Delta\Phi_{\rm exp}$, is approximately equal to $[(23.4^\circ)^2 - (20^\circ)^2]^{1/2} \simeq 12^\circ$.

Cubic insulin triplet phases that were measured for a different project were used to verify the 12° estimated uncertainty. Cubic insulin crystals were grown by button dialysis of 0.018 g zinc-free insulin in 0.05 M Na_2HPO_4 with a dash of Na_2EDTA and traces of NaOH to adjust the pH to 11 against a dialyzing solution of 0.12 M Na_2HPO_4 adjusted to pH 9.2. Data were collected from six large crystals of high perfection (∼1 mm^3, FWHM $\simeq$ 0.005°, space group $I2_13$, a = 78.9 Å). Our strategy focused on measuring triplets where **h**, **g** and **h** − **g** were semi-invariant with only two possible phase values. The triplet phases also had only two possible phase values and consequently could be known exactly since an error of 180° is extremely unlikely (no triplet discrepancy over 100° was ever observed; see Fig. 5). A total of 55 semi-invariant cubic insulin triplets were measured. The interference data for these known triplets was input to computer phasing software that does not enforce the centric phase restrictions. The average difference between the computer phases and the known 'true' phases was 8.2°. The phasing software compares the experimental profile against theoretical profiles in 15° increments, so that possible values are 0, 15, 30° *etc*. This will tend to increase the phasing accuracy since the 'true' phases are semi-invariant and all lie exactly on one of the 'checked' values. We corrected for this by assuming a normal distribution of the errors. There were 28 computer phases with 0° error, 24 with 15° error and three with 30° error. The three computer phases with an error of 30° have a frequency of 3/55 = 5.5%, corresponding to 1.92 standard deviations (from tabulated normal distribution values). Since errors over 22.5° will 'snap' to 30° in the program, 22.5° = 1.92σ, and the measurement error corrected for the sampling advantage is 11.7°. The 27 computer phases with an error of 15° or more have a frequency of 27/55 = 49.1%, or 0.69σ, so 7.5° = 0.69σ and the corrected measurement error is 10.8°. The average of 11.7° and 10.8° is 11.3°, in good agreement with the 12° estimate from the simulations. The expected mean error α is proportional to the standard deviation σ, but the mean error is smaller by $\alpha = \sigma(2/\pi)^{1/2}$, which is 9°. This 9° error estimate for the semi-invariant cubic insulin triplets is less than the 12° error estimate we make for rhombohedral insulin triplets.

Table 2
Quality indicators improve during insulin refinement.

For each refinement stage, the value of each quality indicator and the improvement from the previous refinement stage is shown. The reciprocal-space R factors and improvements are shown in the leftmost two columns of (*a*) (R). The rightmost two columns of (*a*) show the same reciprocal-space R factors, but only reflections for which triplet-phase data were available are considered ($R_{\rm subset}$). In (*b*), the rightmost two columns show the differences between the experimental triplet phases and the triplet phases calculated from the model, $\Delta\Phi$, and the improvement $\Delta\Delta\Phi$. The rightmost two columns show the estimated individual phase error, $\Delta\varphi$, and the improvement $\Delta\Delta\varphi$. Individual phase errors were estimated by subtracting 12° of experimental error and assuming that errors in **h**, **g** and **h** − **g** contribute equally.

(*a*) R factors (%).

	R	ΔR	$R_{\rm subset}$	$\Delta R_{\rm subset}$
Starting model	37.6		32.8	
Atomic ref.	25.2	12.4	25.5	7.3
Water building	22.0	3.2	21.9	3.6
Flat solvent	20.2	1.8	15.9	6.0
DMF	18.4	1.8	12.7	3.2
Alternate conformations	17.8	0.6	12.0	0.7

(*b*) Triplet phases (°).

	$\Delta\Phi$	$\Delta\Delta\Phi$	$\Delta\varphi$	$\Delta\Delta\varphi$
Starting model	39.3		21.6	
Atomic ref.	28.1	11.2	14.7	6.9
Water building	27.2	0.9	14.1	0.6
Flat solvent	24.6	2.6	12.4	1.7
DMF	24.2	0.4	12.1	0.3
Alternate conformations	23.4	0.8	11.6	0.5

Triplet phase data from guinea-fowl hexagonal lysozyme and from *C. thermocellum* endoglucanase were recently reported with a very small discrepancy between measured and calculated phases (Mo *et al.*, 2002). The authors report an average discrepancy of 17.9° for 20 interpretable triplets from lysozyme crystals and an average discrepancy of 15.9° for 40 interpretable profiles from endoglucanase. As in our work, these discrepancies must account for measurement errors and for errors in the refined protein models. It is reasonable to conclude that the contribution from measurement error was of the order of 12° or less in these experiments also. Measurements were made with equipment and methods very similar to those used in this work and these very low phase discrepancies underscore the high precision of measured triplet phases.

3.4. Estimating individual phase errors

Individual phase errors were obtained from triplet-phase differences by removing the estimated 12° experimental error from the known discrepancy between measured and calculated triplet phases and by assuming that the average contributions from **h**, **g** and **h** − **g** were equal. The estimated individual phase error was reduced from $\{[(28.1^\circ)^2 - (12^\circ)^2]/3\}^{1/2}$ = 14.7° to 11.6° during solvent refinement. This 3.1° improvement was partitioned into the contributions from

[1] Simulated data with less noise than our data (4% R factor) resulted in a triplet error of 19°, while simulated data with a noise greater than our data (8% R factor) resulted in a triplet error of 21°. The deduced precision of triplet-phase measurements is 12 ± 2°.

each protocol in conventional *CNS* solvent refinement and from difference-map flattening (Table 2).

3.5. Difference-map flattening solvent improvement

The difference-map flattening (DMF) method was first implemented as a real-space crystallographic refinement procedure for improving the reliability of low-resolution phases (Badger & Caspar, 1991; Badger, 1993). Owing to concerns regarding possible overfitting of the data (Jiang & Brünger, 1994), a smoothing temperature factor is conventionally applied in reciprocal space (Yu *et al.*, 1999) or in real space (Soares *et al.*, 2000). The DMF procedure refines the low-resolution phases by iterative modification of the electron-density map outside the atomic envelope. This yields improved density in the solvent region with a concomitant steep reduction in the data-to-model *R* factors. There are four iterative steps in the DMF procedure.

(i) Calculate a scaled difference map, $\rho(F_{\rm obs}, \varphi_{\rm calc}) - \rho(F_{\rm calc}, \varphi_{\rm calc})$.

(ii) Flatten the difference map (*i.e.* set the density to zero) inside the atomic envelope.

(ii) Smooth the difference map by convoluting with a Gaussian.

(iv) Add the smoothed flattened difference map back into the model map and use the new model map to phase the observed amplitudes and build a new data map.

After two to four iterations of DMF, the solvent region is optimally refined and the data-to-model *R* factors for low-resolution reflections are greatly improved.

4. Results and discussion

The improvements in various measures of the quality of the model at each stage in refinement are shown in Table 2. The conventional reciprocal-space *R* factors and the improvement in the *R* factors with each refinement step are shown in the left pair of columns in Table 2(*a*). Conventional reciprocal-space *R* factors were also computed using only those reflections for which triplet data were available. Those figures are shown in the right pair of columns in Table 2(*a*). The average differences and improvements between observed and calculated triplet phase values are shown in the left pair of columns in Table 2(*b*). The differences and improvements for estimated individual phase errors are shown in the right pair of columns in Table 2(*b*). Individual phase errors were estimated by assuming the errors in the phases of **h**, **g** and **h** − **g** contribute independently and equally to the overall error and by removing the 12° contribution from experimental error in the measurement of the triplet phases (described in §3.3).

The correctness of the atomic model was the dominant contributor to all four measures of model quality, particularly to the reduction in triplet phase errors. Improvement of the atomic model accounted for 63% of the reduction in the conventional *R* factor and for 71% of the overall improvement in the triplet-phase discrepancy. After the atomic model was refined, adding a flat solvent was most effective in reducing triplet-phase errors. Significant improvements were also observed with water building, with difference-map flattening density modification and by modeling alternate conformations of four side chains.

The improvement in the agreement between observed and calculated amplitude data and between observed and calculated triplet-phase data were combined in Fig. 6, where we illustrate an overall summary of the efficacy of each step in the refinement of rhombohedral insulin. Each stage in the refinement results in a model with an associated discrepancy between calculated and measured amplitudes and between calculated and measured triplet phases. Individual phase errors were estimated from the triplet-phase discrepancy as described previously.

In the figure, the average 'true' structure factor is the unit vector along the positive real axis. At its end is an ellipse with height equal to the experimental error in the measurement of triplet phases and with width equal to the average symmetry *R* factor of all reflections for which triplet-phase data were available. This ellipse is the precision of the end point of each individual 'true' structure factor.

The initial model is shown in the figure by a vector with a length that is 32.8% too short and with an angle that is 21.6° away from true, since the initial model had a conventional *R* factor of 32.8% and estimated individual phase error of 21.6°. The final vector is 12.0% too short, with a phase error of 11.6°. Only reflections for which triplet data were available were used in the *R*-factor calculation. The end points of analogously calculated vectors are shown for each stage in the refinement. Each end point is connected, so the vectors shown actually represent the improvement resulting from each stage in the refinement. Of course, ∼50% of the structure factors would

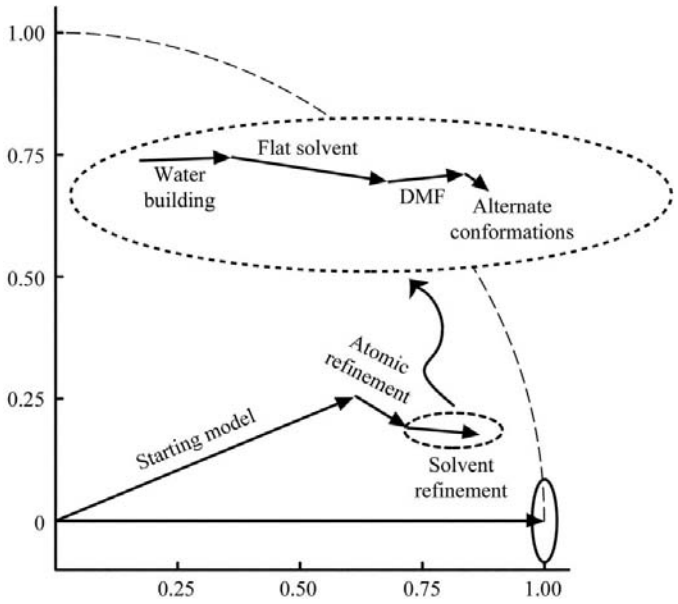

Figure 6
Convergence of amplitudes and phases to experimental values. The figure shows the average relative amplitude and absolute phase difference between experimental values and values calculated from the model at each stage in the refinement. See text for full description.

best be described by vectors that are too long or angles that are negative, but for the figure to be meaningful one direction had to be selected. Similarly, the decision to place the 'true' structure factor on the real axis was arbitrary.

An aggregate measure of the correctness of each model and of the improvement during each refinement stage in Fig. 6 is the distance between the end point of that model's vector and the target point ($x = 1$, $y = 0$). Fig. 7 illustrates the improvement in this quantity and also the improvement in each of its components. Again, a correct atomic model plays a dominant role. Also important is a good overall hydration model, including both ordered water building and an appropriate flat solvent. Further improvement of the hydration model with difference-map flattening and the modeling of alternate conformations were both somewhat effective. One reason for the dominant role played by the atomic coordinate refinement may be that rhombohedral insulin contains only a small fraction of disordered solvent (~25%).

The average difference between experimental triplet phases and model triplet phases prior to DMF was 24.6°. The average improvement subsequent to DMF was 0.4°. At first inspection, the 0.4° reduction in phase error with DMF refinement might appear disappointing. However, the smoothing step in difference-map flattening [step (iii) in §3.5] almost completely suppresses any changes to reflections beyond ~5 Å (at 5 Å, the 50 Å^2 temperature factor suppresses 63% of possible changes). DMF is a fine-tuning step that produces very modest

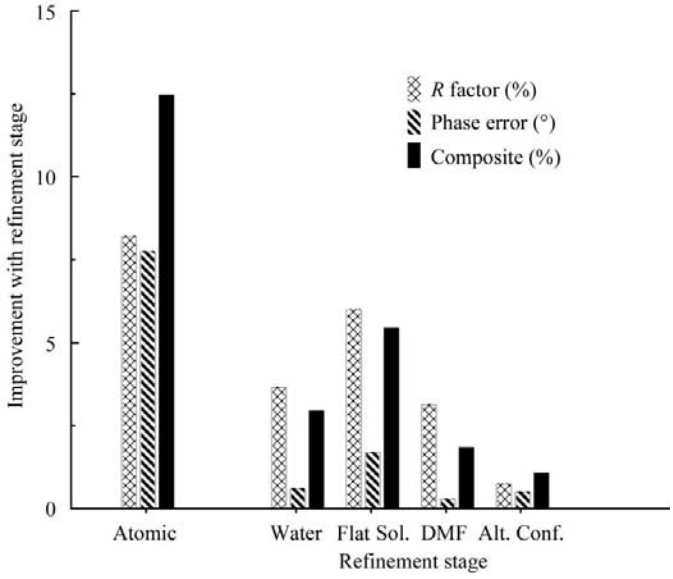

Figure 7
The improvement in various model-quality indicators are shown for each stage in the refinement of rhombohedral insulin. Improvements in the conventional *R* factor (hatched), in the estimated individual phase error (striped) and in the composite indicator (solid) are shown. The composite indicator is the distance between the ($x = 1$, $y = 0$) 'true' position and successive endpoints of the vectors illustrated in Fig. 6. All indicators improve dramatically after atomic refinement, labeled 'Atomic'. This large improvement is shown to the left. The smaller improvements after water building ('Water'), flat solvent incorporation ('Flat Sol.'), difference-map flattening ('DMF') and alternate conformations ('Alt. Conf.') are shown to the right. Only reflections with measured triplet data were included in the conventional *R*-factor calculation.

density changes to the solvent region, which in turn constitutes only 25% of this unit cell. While these density changes are small, in some instances an accurate map in the solvent region may be sufficiently important to warrant the extra effort.

The conventional *R* factor and the triplet-phase discrepancy agree qualitatively in that the model improves during all stages in the refinement of rhombohedral insulin. However, quantitatively the validators do not agree on the relative benefit from each refinement stage. The conventional *R* factor greatly exaggerates the improvement from all refinement outside the atomic envelope. For refinement inside the atomic envelope, the ratio of the improvement in the conventional *R* factor to the improvement in the triplet-phase error is close to 1:1 (12.4% to 11.2°). (This correspondence is fortuitous since the scale is arbitrary, but it provides a reference.) This is also true of the modeling of alternate conformations (0.6% to 0.8°). Outside the atomic envelope the story is very different. The improvement in the conventional *R* factor after water building is 1.8%, compared with a 0.9° improvement in the triplet-phase error, a ratio of 2:1. Density modification fares even worse (1.8% to 0.4°, a ratio of 4:1). Only the adding of a flat solvent avoids this problem, because there are no refined parameters (except the shape of the envelope, which is determined by the atomic structure). In conclusion, the conventional *R* factor overestimates the improvement after refinement outside the atomic envelope, but the triplet-phase discrepancy does not. This is visually apparent in Fig. 6; refinements inside the atomic envelope result in changes directed towards the target, while refinements outside the atomic envelope decrease the closure error but do not point precisely at the target.

Triple-phase invariants determined with multiple-beam diffraction provide an opportunity for testing other low-resolution refinement methods in the same way as they were used here to test DMF. The experimental MAD phases from mannose-binding protein were proposed as ideal for testing models of macromolecular motion and solvation and the methods used to generate those models. Triple-phase invariants are a similar resource, with the benefit that they have a smaller experimental uncertainty and are completely independent of any atomic model.

Experimental problems reduced the initial rate of measurement to 0.25 triplets per hour of beam access. This rapidly improved and has reached an optimal value of two triplets per hour. We find that it is not possible to increase the rate of measurement further without compromising the accuracy of the data using the 'one triplet at a time' strategy. Faster speeds have been achieved using the reference-beam method, raising the possibility of routine phasing of novel macromolecules. Alternatively, refinement against experimental triplet-phase data could reduce the likelihood of error and increase the accuracy of the final atomic model.

Data for this study were measured at beamline X26-C of the National Synchrotron Light Source. Financial support comes principally from the National Center for Research Resources

of the National Institutes of Health and from the Offices of Biological and Environmental Research and of Basic Energy Sciences of the US Department of Energy.

References

Akker, F. van der & Hol, W. G. J. (1998). *Acta Cryst.* D**55**, 206–218.
Badger, J. (1993). *Biophys. J.* **65**, 1656–1659.
Badger, J. & Caspar, D. L. (1991). *Proc. Natl Acad. Sci. USA*, **88**, 622–626.
Blundell, T., Dodson, G., Hodgkin, D. & Mercola, D. (1972). *Adv. Protein Chem.* 279–402.
Brünger, A. (1992). *Nature (London)*, **355**, 472–475.
Brünger, A. T., Adams, P. D., Clore, G. M., DeLano, W. L., Gros, P., Grosse-Kunstleve, R. W., Jiang, J. S., Kuszewski, J., Nilges, M., Pannu, N. S., Read, R. J., Rice, L. M., Simonson, T. & Warren, G. L. (1998). *Acta Cryst.* D**54**, 905–921.
Burling, F. T., Weis, W. I., Flaherty, K. M. & Brünger, A. T. (1996). *Science*, **271**, 72–77.
Chang, S. L., King, H. E. Jr, Huang, M. T. & Gao, Y. (1991). *Phys. Rev. Lett.* **67**, 3113–3116.
Chao, C. H., Hung, C. Y., Huang, Y. S., Ching, C. H., Lee, Y. R., Jean, Y. C., Lai, S. C., Stetsko, Y. P., Yuan, H. & Chang, S. L. (2002). *Acta Cryst.* A**58**, 33–41.
Collaborative Computational Project, Number 4 (1994). *Acta Cryst.* D**50**, 760–763.
Cowtan, K. (1999). *Acta Cryst.* D**55**, 1555–1567.
Cowtan, K. D. & Main, P. (1996). *Acta Cryst.* D**52**, 43–48.
Dodson, E., Kleywegt, G. & Wilson, K. (1996). *Acta Cryst.* D**52**, 228–234.
Engh, R. A. & Huber, R. (1991). *Acta Cryst.* A**47**, 392–400.
Hölzer, K., Weckert, E. & Schroer, K. (2000). *Acta Cryst.* D**56**, 322–327.
Hümmer, K., Schwegle, W. & Weckert, E. (1991). *Acta Cryst.* A**47**, 60–62.
Hümmer, K., Weckert, E. & Bondza, H. (1990). *Acta Cryst.* A**46**, 393–402.
Jiang, J. S. & Brünger, A. T. (1994). *J. Mol. Biol.* **243**, 100–115.
Kleywegt, G. J. (2000). *Acta Cryst.* D**56**, 249–265.
Mo, F., Mathiesen, R. H., Alzari, P. M., Lescar, J. & Rasmussen, B. (2002). *Acta Cryst.* D**58**, 1780–1786.
Mowbray, S. L., Helgstrand, C., Sigrell, J. A., Cameron, A. D. & Jones, T. A. (1999). *Acta Cryst.* D**55**, 1309–1319.
Podjarny, A. D. & Urzhumstev, A. G. (1997). *Methods Enzymol.* **276**, 641–658.
Rice, L. M. & Brünger, A. T. (1994). *Proteins*, **19**, 277–290.
Shen, Q. (1998*a*). *Phys. Rev. B*, **59**, 11109–11112.
Shen, Q. (1998*b*). *Phys. Rev. Lett.* **80**, 3268–3271.
Shen, Q. (1999). *Phys. Rev. Lett.* **83**, 4784–4787.
Shen, Q., Kycia, S. & Dobrianov, I. (2000). *Acta Cryst.* A**56**, 268–279.
Shen, Q. & Wang, J. (2003). *Acta Cryst.* D**59**, 809–814.
Soares, A., Min, J., Bhyrabhatla, B. & Caspar, D. (2000). *Biophys. J.* **78**, 287A.
Terwilliger, T. C. & Berendzen, J. (1999). *Acta Cryst.* D**55**, 1872–1877.
Weckert, E., Hölzer, K., Schroer, K., Zellner, J. & Hümmer, K. (1999). *Acta Cryst.* D**55**, 1320–1328.
Weckert, E. & Hümmer, K. (1990). *Acta Cryst.* A**46**, 387–393.
Weckert, E. & Hümmer, K. (1997). *Acta Cryst.* A**53**, 108–143.
Wlodawer, A., Savage, H. & Dodson, G. (1989). *Acta Cryst.* B**45**, 99–107.
Yu, B., Blaber, M., Gronenborn, A. M., Clore, G. M. & Caspar, D. L. (1999). *Proc. Natl Acad. Sci. USA*, **96**, 103–108.